Chapter 26

Identifying the Spatial Distribution of Vitamin E, Pulmonary Surfactant and Membrane Lipids in Cells and Tissue by Confocal Raman Microscopy

J. Renwick Beattie and Bettina C. Schock

Summary

Every organ compromises of several different cell types. When studying the effects of a chosen compound within this organ or tissue uptake, localisation, metabolism, and the effect itself can be expected to differ between cells. Using the example of Vitamin E in pulmonary tissue we introduce confocal Raman Microscopy as a superior method to localise lipid-soluble compounds within tissues and cells. We describe the analyses of vitamin E, its oxidation products, and metabolites as well as pulmonary surfactant phospholipids in fixed lung tissue sections. Examples of main structural membrane lipids (PC, cholesterol) and an example of a lipid-signalling molecule (ceramide) are also included. Confocal Raman microscopy is a non-destructive optical method of analysing chemical and physical composition of solids, liquids, gases, gels, and solutions. The method is rich in information allowing discrimination of chemically similar molecules (including geometric isomers) and sensitive monitoring of subtle physical interactions. Additionally, Raman spectroscopy is relatively insensitive to water allowing the analysis of aqueous solutions and suspensions typical in biochemistry. In contrast, Raman spectroscopy is sensitive to non-polar molecules making it ideal for lipidomics research.

Key words: Raman Microscopy, Cell Imaging, Membrane Lipids, Vitamin E, Surfactant lipids, Subcellular lipid distribution, Lipid metabolites, Lipid signalling

1. Introduction

1.1. Localisation and Distribution of Molecules Within Tissues and Cells

Every organ compromises of different cell types with specialised function. The lung, for example, has over 30 different cell types and some of these cells, such as alveolar type-II cells are known to have a higher content/uptake of alpha-tocopherol (αT), a form of vitamin E, than, for instance, alveolar type-I cells or bronchial epithelial cells *(1–3)*. Furthermore, tocopherols are differentially

Donald Armstrong (ed.), *Lipidomics,* Methods in Molecular Biology, vol. 579,
DOI 10.1007/978-1-60761-322-0_26,

metabolised depending on the cell type *(4, 5)*. Differential uptake and metabolism of a compound are of particular interest when investigating its therapeutic potential.

Using Raman microscopy we are able to localise different molecules in a tissue section and to determine cell-specific uptake of compounds, their localisation, and metabolism. Identifying the spatial distribution and sub-cellular localisation and metabolism provide important information additionally to the overall (e.g. anti-inflammatory, anti-proliferative, or pro-apoptotic) effect. For instance, the phospholipid structure (e.g. saturated or unsaturated PC) can have a significant impact on the drug–cell interaction as shown for nystatin, an antifungal drug *(6)*.

Conventionally, the effects of nutrients, supplements, or drugs are tested by analyses of the compound within a whole tissue, but its spatial distribution is generally not investigated. In the case of tocopherols, uptake and metabolism can be determined using specially labelled compounds (e.g. deuterated tocopherols) *(7, 8)*. For instance, when rats with experimental acute lung injury inhaled αT, a reduction of some major pro-inflammatory cytokines (proteins and mRNA) was observed *(9)* confirming the overall immunomodulatory effect of αT. However, the cells were mostly affected by αT have not been investigated. Similarly, aerosolised αT in an animal burn and smoke inhalation injury model improved the pulmonary gas exchange *(10)*, an effect that has also been observed using nebulised albuterol or anticoagulants *(11, 12)*.

Aerosol delivery is a specific and fast way to administer agents to the lungs and into the pulmonary circulation. In any case, knowledge about the cell-specific uptake, metabolism, and potential interference with co-localised compounds is of great importance to exclude adverse effects of any therapeutic agent. This will be of particular significance in the light of new developments into personalised drug therapy.

In this chapter we will introduce confocal Raman microscopy to localise lipid-soluble compounds within tissue, especially lung cells and tissue. We shall be using the example of measuring vitamin E, its oxidation Products, and metabolites as well as pulmonary surfactant phospholipids in fixed lung tissue sections. Examples of main structural membrane lipids (PC, cholesterol) and an example of a lipid-signalling molecule (ceramide) are also included.

1.2. Membrane Lipids

Lipids in eukaryotic cells have several very different functions: storage of energy, formation of barriers (cellular membranes), active transport of molecules and ions, and signal transduction messengers *(13)*. The major lipids in eukaryotic cell membranes are glycerophospholipids, sphingolipids, and cholesterol, with phosphatidyl-choline (PC) accounting for over 50% of the

phospholipid fraction. The lipid composition and saturation of the acyl chain of the membrane as well as the cholesterol content determines its fluidity, which is important for membrane protein function (eg. recepters) and may also affect the membranes interaction with drugs *(6)*.

Phospholipids that occur in smaller quantities in the membrane are as important. For example, phosphatidyl-ethanolamine (PE) has a smaller sized polar head group, which when PE is included into the PC bilayers causes a curvature stress onto the membrane. This is important for budding, fission, and fusion *(14)*, as well as major components of vital cell functions such as apoptosis, proliferation, phagocytosis, and secretion. Bioactive lipids such as eicosanoids and sphingolipids are key signalling and regulatory molecules. Ceramide is considered the "central hub" of sphingolipid metabolism and mediates many cell stress responses including differentiation, cell senescence, inflammation, and apoptosis *(15)*. For instance, ceramide accumulation is associated with upregulation of cyclooxygenase (COX)-2 and prostaglandin E2 (PGE2) in aged mice *(16)*. Recently Teichgräber et al. reported that ceramide accumulation in murine cystic fibrosis (CF) cells contributes to the chronic pro-inflammatory state of CF epithelial cells *(17)*. Indeed, using Raman microscopy we show a more varied distribution in human epithelial CF cells **(Fig. 5**).

1.3. Pulmonary Surfactant

Pulmonary surfactant is produced by alveolar type-II cells in the alveoli. It is a complex mixture of lipids and proteins that forms a surface-active film at the air–liquid interface of alveoli and is capable of reducing the surface tension to nearly 0 mN/m. In the upper airways it may function as a lubricant between the sol and gel phase of the airway mucus. Human pulmonary surfactant contains approximately 70% saturated and unsaturated PC, 10% phosphatidyl glycerol (PG), 10% surfactant-associated proteins, and 3% cholesterol. The remaining mass is made up by other phospholipids *(18)*. Saturated PC at room temperature is more gel like, while the addition of unsaturated PC or cholesterol makes the surfactant film more liquid or fluid. Such changes in the surfactant composition can occur rapidly in response to environmental stresses and occur physiologically in heterothermic animals *(19)*. During acute lung injury, cholesterol and protein concentrations increase in lung lavage fluid of rats *(20)* and *in vitro* studies have shown that increasing the cholesterol concentration in pulmonary surfactant above the physiological levels (e.g. to 20%) abolishes surfactant functions *(20, 21)*.

1.4. Vitamin E

Alpha-tocopherol (5,7,8-trimethyltocol, αT) is the predominant form of vitamin E in mammals and while it has other biological roles, its importance originates from its radical scavenging activity:

the chromanol ring reacts with lipid peroxyl radicals to form an oxidised α-tocopheroxyl free radical thereby inhibiting the propagation of those radicals and stabilising polyunsaturated fatty acids in lipoproteins and cell membranes and therefore reduces the release of arachidonic acid from the membrane and its metabolism to prostaglandins *(22–24)*.

In the lung, αT concentrations are tightly regulated through active uptake and secretion by alveolar type-II cells *(2, 3)* and αT is concentrated within the surfactant containing lamellar bodies *(1)*. In the extracellular space it is present at the air–liquid interface as part of the surfactant phospholipid bilayer acting as a first line of defence against inhaled reactive oxygen species. Here it may protect surfactant lipids from peroxidation *(25–27)* and may reduce the oxidative stress onto the underlying cells. Using Raman microscopy and HLPC–EC analyses we found that an exogenous surfactant preparation (BLES™) normally used in newborns suffering from respiratory distress syndrome contains 0.066 ± 0.019 and 0.059 ± 0.014 nmol αT/mg PL, respectively. Work by Atkinson and co-workers indicate that tocopherols may enhance curvature stress or even counteract similar stresses generated by other lipids *(28)*. If so, tocopherols such as αT may play a critical role in vital cell functions where budding, fission, or fusion is involved and knowledge of its concentrations and distribution in the membrane would be crucial to confirm its biological impact. However, it is unknown if αT exhibits any additional therapeutically benefit in the surfactant preparations. Similarly, very little is known about the concentration, distribution, and function of αT in lipid rafts. Cushieri et al. showed that αT-succinate inhibits endotoxin-mediated transport of phosphates to lipid rafts, which provides an alternative explanation of the anti-inflammatory action of αT *(29)*.

1.5. Analyses of Lipids and Lipid-Soluble Compounds

Generally, identification of lipids and lipid-soluble membrane components (such as vitamin E) in biological samples involves the extraction of such with organic solvents *(30, 31)* and the addition of antioxidants (e.g. butylated hydroxytoluene or ascorbic acid) to prevent oxidation of the analyte during processing. Traditional lipids were analysed using thin-layer chromatography (TLC), were a mixture of extracted lipids separated by different adsorption to the solid phase due to their different solubility in the solvent. The same principle applies to any column chromatography and the latter, especially high-pressure liquid chromatography (HPLC), has now replaced most of the TLC analyses. However, there are many advantages of using TLC (which cannot be discussed here) and in skilled hands the methods is still very useful. Similarly to

membrane lipids, pulmonary surfactant lipids can be analysed using these methods.

Vitamin E is most commonly analyzed using HPLC with electrochemical (EC), fluorescence, or UV detection *(32, 33)* or liquid chromatography–mass spectroscopy (LC–MS) *(34)*. HPLC–EC has a sensitivity in the nmol range *(32)*, while mass-spectroscopic methods are more sensitive (LC–MS, pmol range *(35)*). However, the concentrations of metabolites, nitration, or oxidation products together with αT add valuable information about the redox balance in biological samples, but their determination requires separate isolation and analyses *(35, 36)*.

It is important to note that the determination of the concentration of αT or membrane lipids in specific cells or cell fractions (e.g. mitochondrial membranes) requires the application of stringent laborious isolation procedures *(37, 38)*. This approach, however stringently and precisely it is performed, has still one major disadvantage when studying biological effects on cells and tissues; namely having to extract the lipid-soluble compounds in order to quantify them will exclude vital information about its spatial distribution from the investigator. While metabolites may be analysed separately, no information can be obtained about the co-localisation with other (lipid-derived) compounds or those involved in metabolism. Furthermore, separate extractions and analyses may be rather time consuming reducing the applicability to follow kinetics of uptake and metabolism, again especially with co-localisation of other lipids of interest.

Other methods involve labelling of lipid membrane-associated proteins using e.g. fluorescence antibodies. However, using confocal laser scanning microscopy, this would only "indirectly" identify functional groupings such as lipid rafts *(39, 40)*. Antibodies against αT and cholesterol (USBiological, Antibodies-online GmbH, Germany) *(41)* have been developed, but their reactivity with "free" αT or steroid is poor. Recently, time-of-flight secondary ion mass spectrometry (TOF-SIMS) was used to visualise a number of lipid compounds, including vitamin E *(42)*. While TOF-SIMS achieved similar levels of spatial resolution to Raman Microscopy (around 1 μm), it, like all other methods mentioned above, destroys the sample.

1.6. Raman Spectroscopy

Raman spectroscopy analyses the vibrations of a molecule after excitation with monochromatic (laser) light. The amount of energy removed from the incident light is directly related to the chemical structure as well as any intra- or intermolecular interactions that may affect the freedom of this vibration. The light scattered from the sample is collected and separated into different energies giving a Raman spectrum, which is rich in information on both the chemical and physical properties of the sample. Con-

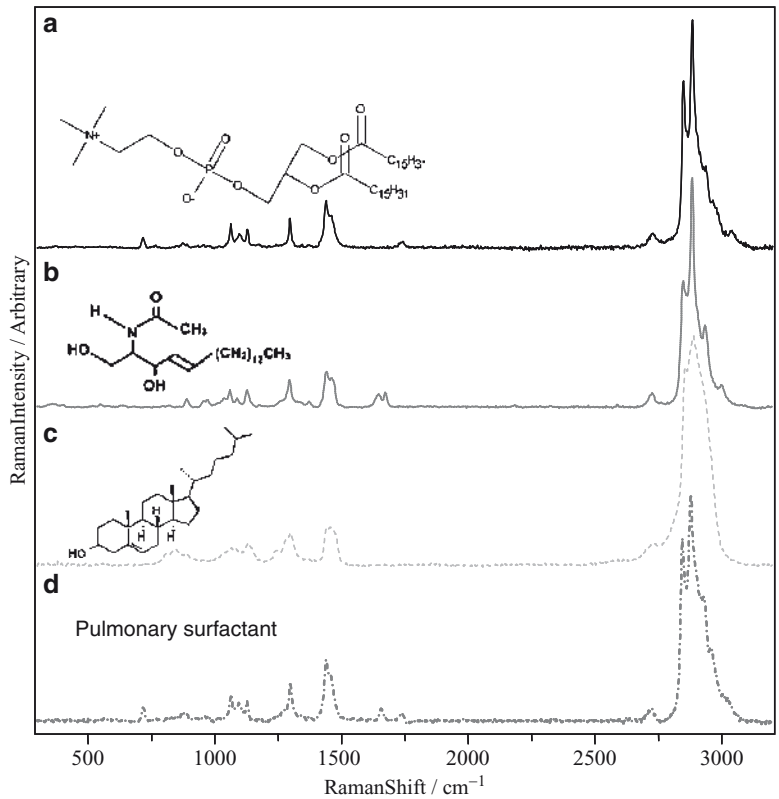

Fig. 1. Raman spectra (633 nm excitation) and chemical structures of some main exemplary structural membrane lipids: (**a**) DPPC, (**b**) Ceramide (C2-ceramide) as ana example of a lipid signalling molecule, (**c**) Cholesterol, and (**d**) Pulmonary surfactant (BLES™, lung surfactant extract).

sequently Raman spectroscopic methods have been extensively applied to the study of a wide range of lipid systems including fatty acid analysis, essential oils, and hydrophobic vitamins *(1, 43–46)*. **Figure 1** shows the Raman spectra of selected lipid compounds that play a major role in lipid membranes and physiological surfactants.

The discrimination power of Raman spectroscopy is briefly illustrated in **Fig. 2**, which shows the Raman signals obtained from neat samples of four tocopherolic compounds. Indicated by arrows are a number of changes in the Raman spectrum that are a direct consequence of the changes in molecular structure. For example, γT is identical to αT except that it lacks a methyl group at the top of the aromatic ring (position 5), and this difference results in the disappearance of the αT mode at 485 cm^{-1}. The 2 e^- oxidation product, αTQ differs in that the chromanol ring has been destroyed and replaced by a quinine group, and this is

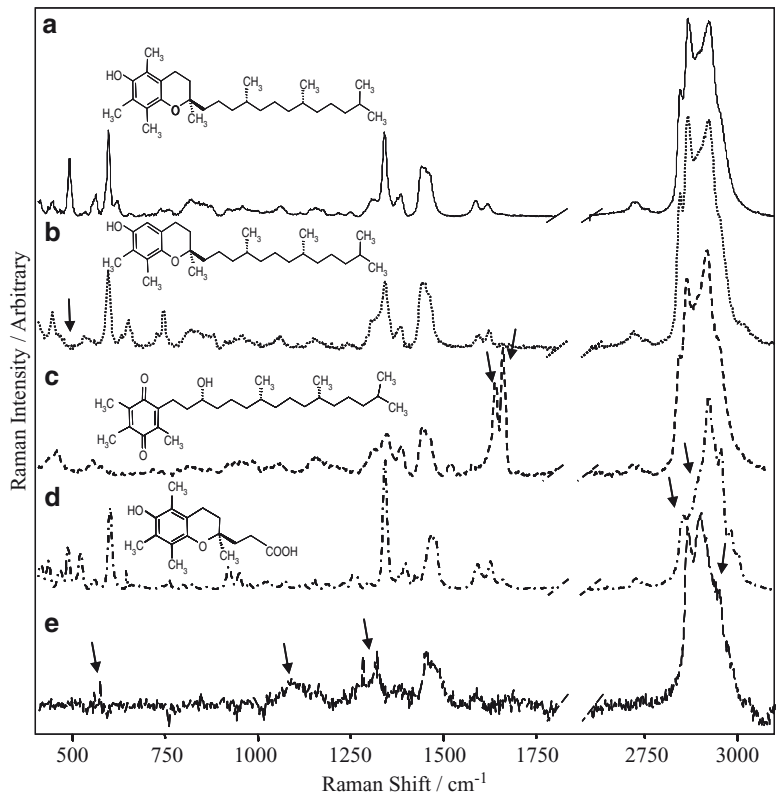

Fig. 2. Raman spectra (633 nm excitation) and chemical structures of chromanol molecules (**a**) α-tocopherol (**b**) γ-tocopherol (**c**) α-tocopherol quinone (**d**) α-3′-carboxyethylhydroxychromanol (α-CEHC) and (**e**) α-tocopherol in cell homogenate. Significant changes in the Raman signal, of α-tocopherol quinone, compared to α-tocopherol, are indicated by *arrows*, and these changes can be directly related to the change in the chemical structure.

reflected in the Raman signal by the loss of the doublet at 1,585 and 1,615 cm^{-1} and the appearance of a much stronger doublet at 1,633 and 1,655 cm^{-1}. The 1 e^- oxidation product of αT has had the phytyl chain removed and replaced by an acid group, resulting in the disappearance of the strong doublet at 2,845 and 2,865 cm^{-1}, which is a characteristic doublet of extended branched aliphatic chains. **Table 1** summarises the typical Raman shifts for a range of common lipid molecules *(1, 47–51)*.

In addition to the high information content, Raman spectroscopic methods offer many further benefits. For example, it is non-destructive and water is a very weak Raman scatterer allowing analysis in aqueous environments. Additionally the optical nature of the Raman methodology allows it to be combined with a very wide range of standard microscopic procedures and therefore allows the method to be incorporated very non-invasively into an existing experimental setup. All that is required is that the

Table 1
Some Raman band assignments for common moieties in lipids *(1, 47–51)*

Band position	Assignment	Notes
3,100–3,600	OH	Sensitive to hydrogen bonding strength
3,060	CH stretch	Sensitive to conjugation and geometric isomers
3,030	CH_3 stretch	In choline headgroup
2,960	CH_3 asymmetric stretch	
2,930	CH_2 asymmetric stretch	Ratio of intensity to mode at 2,850 cm^{-1} is commonly used as a marker of polymethylene chain conformation
2,870	CH_3 symmetric stretch	
2,850	CH_2 symmetric stretch	
1,710–1,750	COOR	Carbonyl stretch in ester, used as molar reference band in fatty esters
1,550–1,700	COO^-, C = O	Position and width dependant on strength of hydrogen bonding
1,670	*Trans* isolated C = C	Correlation between intensity and number of *trans* C = C in molecule
1,660	*Cis* isolated C = C	Correlation between intensity and number of *cis* C = C in molecule
1,630–55	Quinone, conjugated dienes	
1,607–30	Aromatic, conjugated trienes	
1,582–7	Aromatic ring	
1,515–1600	Conjugated C = C,	Length correlated with Raman shift
1,410–1490	CH_2	Decreases with increasing hydrophobicity. Sensitive to intermolecular forces, i.e. crystallinity. Correlates with polymethylene chain length.
1,400–1420	COO^-	Sensitive to hydrogen bonding strength
1,380	CH_3 twist	
1,300	CH_2 twist	Position sensitive to intramolecular forces, i.e. chain conformation. Intensity correlates with chain length
1,250–12,70	=C–H in cis	Band gives very weak intensity for *trans* isomers.
1,260	PO_2^- asymmetric stretch	
1,020–1,130	C–C, N, O stretch.	Sensitive to intramolecular forces. Characteristic pattern of three bands within linear polymethylene chains. Intensity correlates with polymethylene chain length.

(continued)

Table 1 (continued)

Band position	Assignment	Notes
1,090	PO_2^- symmetric stretch	
880–965	C–C	Terminal $H_xC–CH_3$ and C–C adjacent to C = O
875	C–N stretch	Choline group, trans conformation
761	OPO symmetric stretch	Diphospho-ester
720/770	C–N totally symmetric stretch	Sensitive to conformation in the choline headgroup, high Raman shift for *trans*, low for *cis*
<200	Whole molecule	Related to whole molecule motion, translation, rotation, breathing, etc.

Table 2
Advantages and disadvantages of Raman spectroscopic techniques

Advantages	Disadvantages
Minimal interference from water	Weak effect
Non-contact, non-invasive.	Expensive
All physical states of matter	Can be time-consuming
Minimal sample preparation	Hi-tech
Non-destructive	Fluorescence can interfere
Spatial resolution diffraction limited	Processing tools underdeveloped
Measure < 1 pg material	
Rich chemical and physical information content	
Instrumentation highly adaptable	
Special techniques extend: Sensitivity (e.g. Surface Enhanced RS), Specificity (e.g. Resonance RS), Spatial resolution (e.g. Tip Enhanced RS)	

user is able to direct a laser onto the sample and collect the light scattered from it. **Table 2** summarises the key advantages and disadvantages of Raman spectroscopic methods.

These advantages have allowed Raman spectroscopy to be used to investigate a range of tissues both *in vitro* and *in vivo* (52–54).

Combining Raman spectroscopy with optical microscopy offers these advantages on a micron-scale of spatial resolution, without lengthy sample processing and/or the addition of (bio) chemicals.

In order to explore other lipid constituents or lipid bilayers it is not necessary to make changes to the Raman methodology, but calibration with a suitable approach for that constituent and recording its reference Raman spectra under the same conditions is required. It should be noted that sample preparation is not dictated by the needs of the Raman spectrometer, but rather by the conditions under which the sample is in a relevant state. Furthermore, as Raman microscopy can differentiate the main constituents of membrane lipids (sphingolipids, ceramide, cholesterol, PC), the method may also be applied to visualise microdomains such as cholesterol and sphingolipid-enriched lipid rafts. Using water immersion objectives will enable the visualisation of the organisation and interaction with functional proteins within such domains, providing a novel method to study the role of lipid rafts in e.g. endocytosis and membrane signalling *(55)*.

1.7. Multivariate Statistics

Because of the complexity of the information measured by Raman spectroscopic methods, it is commonplace to employ multivariate statistics in order to simplify the data and home in on only the information that is relevant. Qualitative analysis is most commonly carried out using principal component analysis (PCA), which identifies the limited range of basic spectral signals that, in various combinations, account for all the signals within the dataset. The results of most interest from PCA are the basic spectral signals (loadings) and the scores, which reflect the relative contribution of these basic spectral signals to each sample spectrum. Partial least squares (PLS) regression is the most commonly applied quantitative analysis, which correlates the sample spectrum with a reference parameter. The regression coefficients are the spectral bands that were used to correlate with the reference value, and are an excellent way of checking the correlation based on direct spectral measurement of the target analyte. An excellent introduction to multivariate statistics is available from Umetrics AB (Umea, Sweden) *(56, 57)*.

2. Materials

2.1. Equipment

1. Horiba Jobin-Yvon LabRam HR800 Raman confocal microscope. (*see* **Note 1**)
2. A 633-nm excitation laser (10 mW at sample, focused beam diameter <1 μm, *see* **Note 2**).

3. A "window" (range of the spectrum detectable in one acquisition) of 800–3,100 cm^{-1} *see* **Note 3**
4. A 300 groove mm^{-1} diffraction grating (giving 12 cm^{-1} spectral resolution).
5. Microscope objectives (*see* **Note 4**, magnification 10×, 50×, and 100×; e.g. Olympus M-plan NA0.9, confocal hole 600 μm).
6. A 0.1-μm step size motorised, computer-controlled *xyz* stage.
7. Labspec™ (Jobin-Yvon, Villeneuve d'Ascq, France) to record and process the optical and spectral images.
8. Software capable of performing multivariate analyses (PCA, PLS), such as "The Unscrambler" (Camo, Oslo, Norway).
9. A more detailed and technical account of Raman instrumentation is available *(58)*.

2.2. Reagents and Supplies

Pure reference samples for any lipid species to be targeted should be used.

1. DL-alpha-*Tocopherol* and *Cholesterol* (SIGMA, UK).
2. Palmitic acid methyl ester *(PAME)* (SIGMA, UK).
3. Carboxyethylhydroxychromanol, *α-CEHC*.
4. C_2-*Ceramide* (BIOMOL International LP, UK).
5. 1,2-Dipalmitoyl-*sn*-glycero-3-phosphocholine, saturated *DPPC* (Avanti Polar Lipids (no 850355), USA).
6. Bovine lung extract surfactant, *BLES*™ (BLES Biochemical Inc. Canada).
7. CaF_2 microscope slides (Crystrans, Poole, UK, *see* **Note 5**).
8. N_2 (or other inert gas) to flush the sample to prevent oxidation during signal aquisition.
9. Standard methods were applied for cell culture and homogenising of tissue *(1)*.

3. Method

3.1. Calibrating the Raman Signal (See Note 6)

1. First obtain pure reference material for the substances of interest and a sample containing the reference material in the relevant matrix. Record their Raman spectrum; the exact procedure will be dependant on the instrumentation employed.
2. Because Raman spectroscopy is sensitive to physical interactions it is important to measure the reference materials under a range of conditions and within a relevant matrix (*see* **Note 6**). As an example, **Fig. 2a** shows the Raman spectra obtained

from the pure reference material (αT) as well as the reference material in cell homogenate **(Fig. 2e**). Because Raman spectroscopy is based on UV, visible, or NIR radiation it is possible to measure a sample through any substance transparent to the excitation wavelength. This has the consequence that Raman experiments can easily be performed using chambers or incubators that control local environment. This opens the possibility of probing chemical and physical changes occurring in response to temperature, humidity, controlled atmospheres, and pressure.

3.2. Validation of the Spectroscopic Analyses

1. Because we are calibrating a spectroscopic method rather than directly measuring a parameter it would be ideal to prepare a sufficiently large set of samples to allow for a separate calibration and validation set (2:1 ratio of samples). If it is unrealistic to prepare sufficient samples for two sets, then cross validation can be used on a single set of data, though this may have a tendency to be slightly optimistic about model performance. The calibration should be performed over a realistic range of concentrations reflecting the range encountered in vivo (remembering, if the target analyte is likely to be localised, that its local concentration may be greater than the average concentration within the whole tissue).
2. To calibrate the analyses for both the Raman signal within biological matrix and quantification of αT, we supplemented lung epithelial cells in culture with increasing concentrations of αT (0–50 μM, dissolved in ethanol) and determined the αT concentration of a cell homogenate by HPLC-ECD *(1)*. The homogenate should be in the same state as the tissue to be mapped (e.g. wet or dehydrated). A portion of the homogenate (10 μl) was also placed into a 0.8-mm diameter well in CaF_2 or aluminium and dried under N_2.
3. Record Raman spectra from a representative grid over the homogenate and then average the spectra for each sample (*see* **Note 7**). The signal-to-noise ratio (*S/N*) of the band around 2,930 cm^{-1} from the average spectrum of each sample should be at least 50 for the calibration. Remove the background signal from the Raman spectra (*see* **Note 8**), normalise the spectra by dividing each point by the average intensity of the spectrum (*see* **Note 9**) then input the data into the statistical package, along with HPLC-measured parameters.
4. Carry out a PLS regression, incorporating wavelength selection to create a more robust model. Compare the regression coefficients with the spectra of the pure reference compounds as shown in **Fig. 3** (*see* **Note 10**).

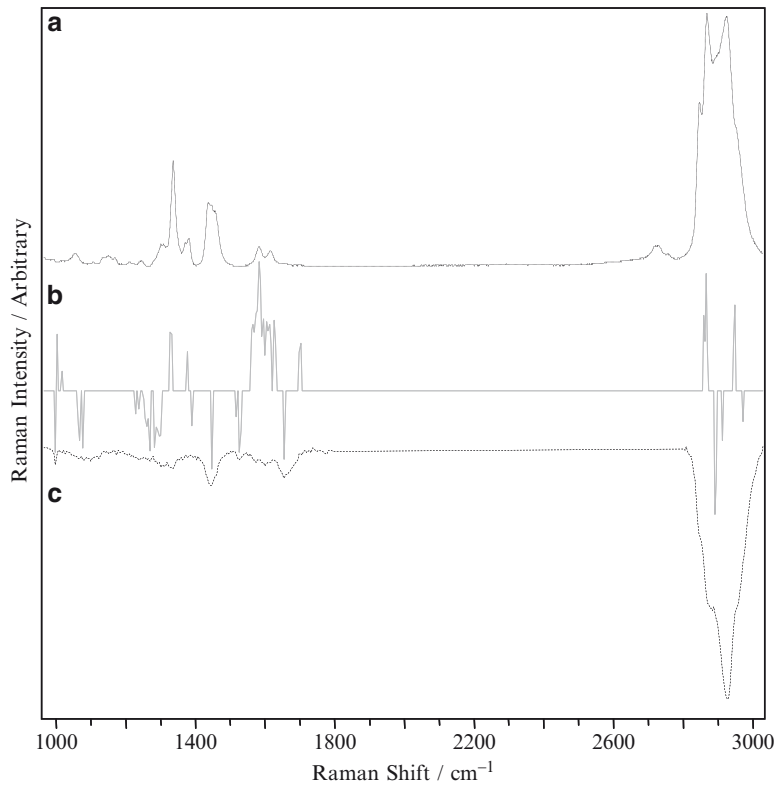

Fig. 3. Interpreting the regression coefficients used in a PLS regression of the Raman signal against HPLC-determined α-tocopherol concentration in A549 cells supplemented with a range of tocopherol concentrations. (**a**) Raman signal of pure α-tocopherol (**b**) regression coefficients used to transform the Raman signal into the predicted α-tocopherol concentration (**c**) the Raman signal of an unsupplemented A549 cells multiplied by –1 for comparison with negative coefficients.

3.3. Acquiring the Raman Data of the Sample

Select a suitable area of the sample. If the target analyte is highly localised it is possible to use a low-spatial resolution (5–10 μm spacing) scan over a large area; follow the remaining procedure and then repeat in higher resolution in an area identified from the initial screen as containing the target analyte. The individual spectra used to quantitatively predict the target analyte should have an S/N of at least 10.

3.4. Qualitative Mapping

1. It is not recommended to normalise the spectral intensity of mapped data before qualitative analysis. Import the data into the statistics package and perform a PCA. Identify principal components (PCs) relating to target analytes by comparing the loadings with the reference spectra recorded initially. These loadings contain a positive and a negative constituent, which can make interpretation difficult. In order to visualise the

spectra related to the component it is necessary to average the most extreme scores and their corresponding spectra for each loading.

2. For the highest rank PCs these spectra will match the signals of the constituents contributing to the PC, but for lower ranked PCs these signals will not necessarily be the dominant band shape within the spectrum. Add the loadings onto the extreme high score spectrum and subtract the loadings from the extreme low score spectra until just before negative bands start to appear in the spectrum. The process is illustrated in **Fig**. **4** and it is clear that the spectral constituents contributing to the PC are easier to identify, allowing the identification of α-tocopherol and α-tocopherol quinone signals in nitrogen-flushed and unflushed tissues, respectively. The scores of the PCs can be mapped using their original coordinates in order to obtain a pseudo-image like those shown in **Fig**. **5a** and **6 e–j**.

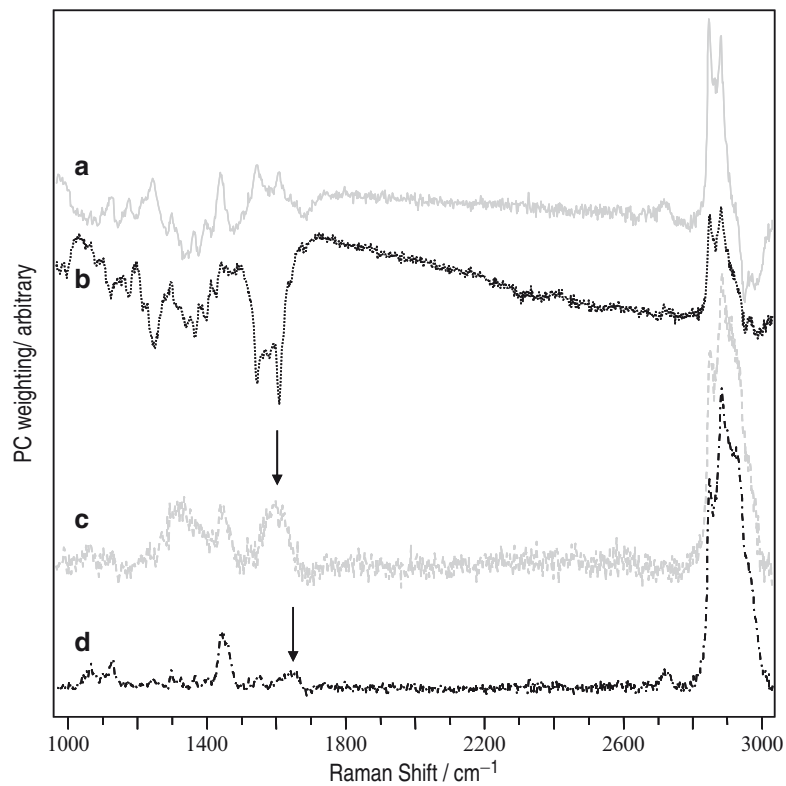

Fig. 4. Extracting spectral signals from PCA. Spectral loadings containing tocopherolic signals from (**a**) N_2flushed lung section and (**b**) unflushed lung section. The negative contributor to the loadings makes it difficult to confidently assign the tocopherol. By adding the loadings to the average high score spectra the tocopherol signals contributing to the high score samples (c + d) are clear. The position of the *arrowed* band in (**c**) matches with that of the aromatic mode in α-tocopherol, while that of (**d**) matches α-tocopherol quinine, indicating that without a N_2 flush, oxidation of the α-tocopherol can occur.

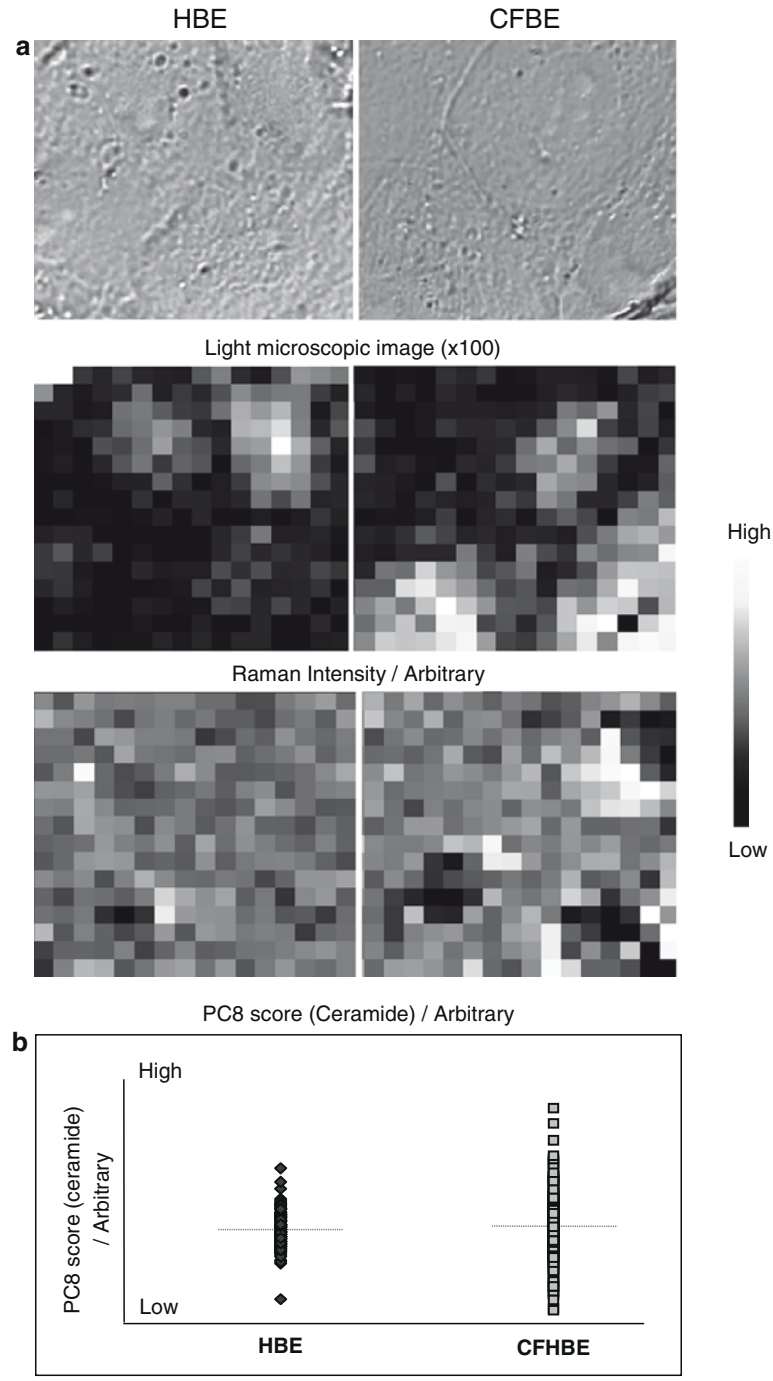

Fig. 5. Raman mapping of human bronchial epithelial cell lines with and without a CFTR mutation (HBE and CFBE, respectively) and PCA analyses for the lipid signalling molecule ceramide. (**a**) The light microscopic image, Raman map (Intensity) and Raman map after processing for PC8 scores (ceramide). (**b**) A summary plot of the PC8 scores for ceramide.

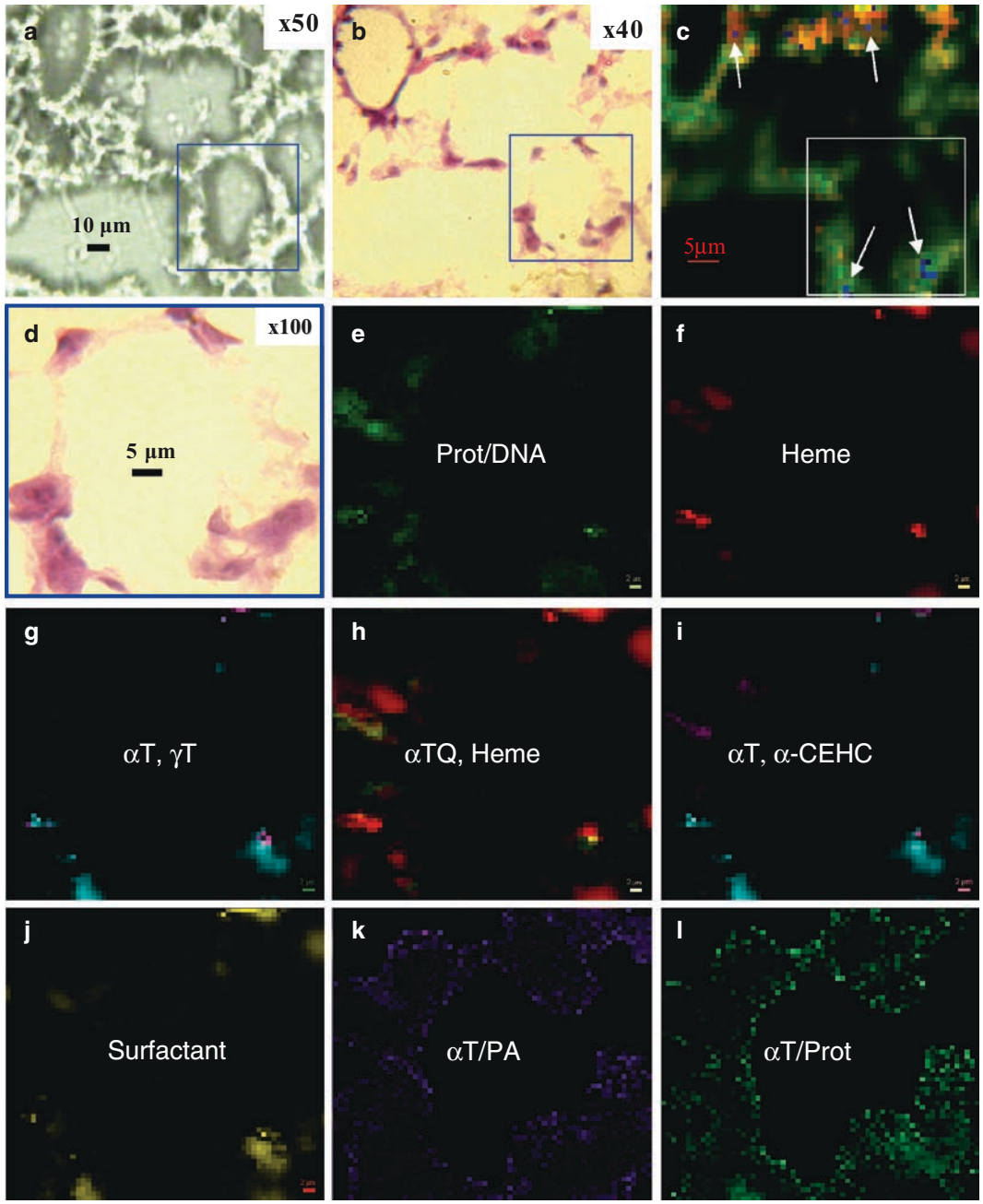

Fig. 6. Raman maps for a number of biochemical constituents identified in mouse lung during PCA. (**a**) Bright-field image of mouse lung at ×50 magnification (10-µm section after fixation with 4% PFA and short-term storage in 5% sucrose). (**b**) Histological appearance of the same mouse lung section after haematoxylin/eosin (HE) staining. (**c**) Raman map with 2-µm spacing of the same mouse lung section (×100) showing nuclear protein (*green*), heme (*red*), and α-tocopherol (*blue*). (**d**) Insert shown in (**b**) at ×100 magnification after HE staining. (**e–l**) Raman maps of the insert shown in (**a**) at 0.8-µm spatial resolution: (**e**) protein/DNA (*green*); (**f**) heme (*red*); (**g**) α-tocopherol (*cyan*) and γ-tocopherol (*magenta*); (**h**) α-tocopherol quinone (*yellow-green* due to overlap with *red*) and heme (*red*); (**i**) α-tocopherol (*cyan*) and α-CEHC (*magenta*); (**j**) pulmonary surfactant (*yellow*); (**k**) α-tocopherol/palmitic acid (*turquoise*); (**l**) α-tocopherol/protein (*green*). **Figure 6a–d** and **g–j** reprinted with permission from ***(1)***.

3.5. Quantitative Mapping

Process the data in the same way as the calibration data was processed but exclude any signals wka signal-to-noise ratio below 10 as these are below detail in limit. Import the data into the statistics package and perform a prediction using the PLS regression model created during the calibration step. Use the original mapping coordinates to reconstruct a pseudo-colour image of the predicted analyte as shown in **Fig. 6k** and **l**.

3.6. Interpretation of Results

1. In order to interpret the Raman spectra from the sample under study, it is essential to have a comprehensive database of representative spectra available for comparison. Use of spectral database software will compare the sample spectrum with the reference spectra and report which reference spectra are most similar to the sample. In some cases it may not be possible to obtain a pure reference spectrum of the target analyte, in which case a spectral database will not be applicable. Alternatively, the sample spectrum can be compared with published spectra, tables of assignment and comprehensive vibrational analyses of related molecules. Despite its age, Tu's book on Raman spectroscopy in biology remains a very comprehensive reference for typical spectral signals of a wide range of biochemicals *(59)*.
2. As mentioned above, it is imperative that physical interactions and states are replicated accurately between the sample for the reference spectrum and the form that is found naturally within the sample. In **Fig. 2** spectra ***a*** and ***e*** compare aT in the neat liquid and in association with cells, and it is clear that the physical interactions within the cells cause measurable changes in the Raman spectrum. Understanding the relationship between physical interactions and the Raman signal of lipids allows careful probing of lipid structure in membranes as well as chemical composition *(60)*.
3. Because of the close link between the Raman spectrum and the chemical structure of the analyte it is possible to speculate on the origin of an unidentified signal. If a reference sample of the suspected molecule is obtained then it can be accounted for in the original data without the need to re-record the sample data *(61)*.
4. Raman spectroscopic methods are a point of focus method and the intensity of light scattered from the sample is affected by a vast range of interferences *(58)*. It is therefore important to understand the principal source of signal variation in the data. When mapping a small area of a sample relatively quickly as in *(1)*, the principal source of intensity variation is likely to be due to the absolute amount of molecules in the sampling volume – but will also be sensitive to the morphology of the sample. In **Fig. 5** we show the absolute Raman signal of ceramides in human bronchial epithelial cells using

the widely used cell lines HBE and CFBE (D. Gruenert, San Francisco, USA). Raman microscopy shows a more varied distribution in the CF cell line, which may suggest that these cells are in a higher activation state as increased incorporation and movement of ceramides within lipid rafts is required for bacterial internalisation, induction of apoptosis, and controlled release of cytokines and membrane receptor activation. In **Fig. 6** the maps ***c–j*** are constructed from the PCA scores of non-standardised spectra, and consequently they reflect the absolute number of each molecule with the sampling volume at each point. Thus the concentrations of most materials appear higher in the centre of cells due to the fact there is more material there than at the edge. However, it is rarely the case that the absolute number of moles is of interest, but rather the concentration of the analyte with respect to its matrix or to another constituent. For quantitative analysis by Raman spectroscopy it is imperative that the data is appropriately normalised *(62)*. **Figure 6** maps ***k*** and ***l*** show the distribution of αT relative to protein and surfactant, respectively. It is clear that by ratioing the analyte signal to another constituent, a completely different type of information is gained. Comparison of **Fig. 6g** (αT in cyan) with *j* and ***k*** shows that although the largest total amount of αT molecules is in the centre of the cell, when expressed relative to the surfactant the concentration appears to be higher in the lining of the alveolus, the site of highest oxidative stress.

4. Notes

1. For larger samples (e.g. 100 μl of extracted material) a macro Raman instrument is preferable, with spot sizes available from 50 to 500 μm in diameter. For discussion on the relative merits of micro- and macro-Raman instrumentation, *see (60)*.
2. For fluorescent samples use of 785-nm excitation is typically recommended. For non-fluorescent samples 633 nm offers the benefit of enhanced Raman scattering efficiency, optical transmission, and detection efficiency as well as allowing use of extra-white glass as a substrate if cost is an important consideration. Accurate measurement of beam diameter is essential for determining spatial resolution. Measure the Raman spectrum along a line projecting over the vertical edge of a silicon wafer and measure the distance between 95 and 5% signal intensity – this distance represents the 2-standard deviation diameter of the beam intensity.
3. The size of the spectral window is inversely related to the spectral resolution of the instrument.

4. For tissue mapping or low volume extracts a confocal Raman microscope is required, allowing measurement from volumes of the order of 1 μm^3, <1 pg of material (*see* **Note 2**). When using a high magnification objective, a water immersion lens is required for use on hydrated samples to avoid refraction problems at the sample surface. Raman methods can be easily incorporated into a plethora of configurations, allowing the sample to be probed under almost any condition imaginable. Use of water immersion objectives or an inverted configuration immediately opens the possibility of probing living tissue and cells. Phase contrast Normaski and other contrast enhancing methods can be incorporated to help the user visualise unstained biological materials, making the selection of analysis area easier.
5. The main issues associated with choosing a suitable substrate for the sample are minimal spectral features and as low a broadband signal as possible. CaF_2 slides give a very low background, with a single sharp peak around 325 cm^{-1}, making them an ideal substrate for many applications, but are expensive. If high throughput demands a cheaper alternative extra white slides (Menzel-Gläser, Braunschweig, Germany) give a much higher background than CaF_2, but when compared with quartz these have smaller spectral features but comparable intensity of broadband background. Standard glass gives broadband signal intensity around three times that of extra white glass. However, if the excitation wavelength is in the NIR (>750 nm) then glass (standard or extra white) gives a very strong emission that swamps the Raman signal so that CaF_2 or quartz must be employed.
6. It is important to design the calibration to measure the analyte in relevant circumstances. Supplementation studies ensure biological relevance, but the cell lines used must have biochemical properties similar to the situation in situ. For example, two calibrations allow prediction of aT/protein and aT/surfactant ratios. Supplemented (alveolar type II-cells A549) created a prediction of aT/protein ratio. A separate calibration of standardised mixtures of aT and palmitic acid methyl ester were used to create a prediction of aT/surfactant ratio. In this later situation the dominance of palmitic acid in lung surfactant allowed modelling using a simpler and cheaper system, but using pulmonary surfactant instead of palmitic acid would also be valid.
7. It is most useful to record multiple (minimum ten for confocal microscope systems) spectra from different regions of the sample to check for consistency. PCA will highlight any deviations such as impurities, polymorphism, or domain formation. Using this approach any detectable impurities can be eliminated from the signal post acquisition, leaving the pure signal of the target analyte.

8. The raw data acquired from a Raman experiment is not a pure Raman spectrum, but contains contributions from optical phenomena other than Raman, such as fluorescence. For this reason it is necessary to eliminate this low information broadband signal from the data set prior to quantitative analysis. A large number of methods exist, with excellent review available in *(63)* and some promising new automated methods *(61, 64)*.
9. The absolute Raman intensity is very difficult to measure reproducibly, being dependant on a very large number of factors *(58, 62)* and for this reason it is necessary to standardise the intensity prior to quantitative analysis.
10. The positive bands in the regression coefficients should match distinctive bands in the target analyte, while the negative bands should match distinctive bands in the cells or tissue under study. If the bands do not match those in the reference material, the model is depending on a cross correlation that may not apply in independent samples. Wavelength selection ignores Raman shifts that are unreliable for predicting the target analyte, either because the target analyte shares intensity with the cell or because there is a third constituent unrelated to the analyte.

Acknowledgement

Research was supported by a grant from the BBSRC, UK (JREI 18471) and the R&D Office, Northern Ireland (SPI/2384/03). JRB is supported by a grant from the Medical Research Council (MRC), UK (G0600053). The authors thank Mr. C. Maguire for technical support. BLES™ was a gift from BLES Biochemicals Inc., Canada (H. Dick) and the tocopherol metabolite was a gift from F. Galli and F. Mazzini (University of Perugia, Italy). The authors are very grateful for these contributions.

References

1. Beattie, J.R., Maguire, C., Gilchrist, S., Barrett, L.J., Cross, C.E., Possmayer, F., Ennis, M., Elborn, J.S., Curry, W.J., McGarvey, J.J., and Schock, B.C.,(2007) The use of Raman microscopy to determine and localize vitamin E in biological samples. *FASEB J.* **21**, p. 766–76.
2. Kolleck, I., Schlame, M., Fechner, H., Looman, A.C., Wissel, H., and Rustow, B.,(1999) HDL is the major source of vitamin E for type II pneumocytes. *Free Radic Biol Med.* **27**, p. 882–90.
3. Hosomi, A., Goto, K., Kondo, H., Iwatsubo, T., Yokota, T., Ogawa, M., Arita, M., Aoki, J., Arai, H., and Inoue, K.,(1998) Localization of alpha-tocopherol transfer protein in rat brain. *Neurosci Lett.* **256**, p. 159–62.
4. You, C.S., Sontag, T.J., Swanson, J.E., and Parker, R.S.,(2005) Long-chain carboxychromanols

are the major metabolites of tocopherols and tocotrienols in A549 lung epithelial cells but not HepG2 cells. *J Nutr.* **135**, p. 227–32.

5. Jiang, Q., Freiser, H., Wood, K.V., and Yin, X.,(2007) Identification and quantitation of novel vitamin E metabolites, sulfated long-chain carboxychromanols, in human A549 cells and in rats. *J Lipid Res.* **48**, p. 1221–30.
6. Hac-Wydro, K., Kapusta, J., Jagoda, A., Wydro, P., and Dynarowicz-Latka, P.,(2007) The influence of phospholipid structure on the interactions with nystatin, a polyene antifungal antibiotic A Langmuir monolayer study. *Chem Phys Lipids.* **150**, p. 125–35.
7. Galli, F., Lee, R., Dunster, C., and Kelly, F.J.,(2002) Gas chromatography mass spectrometry analysis of carboxyethyl-hydroxychroman metabolites of alpha- and gamma-tocopherol in human plasma. *Free Radic Biol Med.* **32**, p. 333–40.
8. Leonard, S.W., Paterson, E., Atkinson, J.K., Ramakrishnan, R., Cross, C.E., and Traber, M.G.,(2005) Studies in humans using deuterium-labeled alpha- and gamma-tocopherols demonstrate faster plasma gamma-tocopherol disappearance and greater gamma-metabolite production. *Free Radic Biol Med.* **38**, p. 857–866.
9. Hybertson, B.M., Chung, J.H., Fini, M.A., Lee, Y.M., Allard, J.D., Hansen, B.N., Cho, O.J., Shibao, G.N., and Repine, J.E.,(2005) Aerosol-administered alpha-tocopherol attenuates lung inflammation in rats given lipopolysaccharide intratracheally. *Exp Lung Res.* **31**, p. 283–94.
10. Morita, N., Traber, M.G., Enkhbaatar, P., Westphal, M., Murakami, K., Leonard, S.W., Cox, R.A., Hawkins, H.K., Herndon, D., Traber, L.D., and Traber, D.L.,(2006) Aerosolized alpha-tocopherol ameliorates acute lung injury following combined burn and smoke inhalation injury in sheep. *Shock.* **25**, p. 277–82.
11. Enkhbaatar, P., Cox, R.A., Traber, L.D., Westphal, M., Aimalohi, E., Morita, N., Prough, D.S., Herndon, D.N., and Traber, D.L.,(2007) Aerosolized anticoagulants ameliorate acute lung injury in sheep after exposure to burn and smoke inhalation. *Crit Care Med.* **12**, p. 2805–10
12. Palmieri, T.L., Enkhbaatar, P., Bayliss, R., Traber, L.D., Cox, R.A., Hawkins, H.K., Herndon, D.N., Greenhalgh, D.G., and Traber, D.L.,(2006) Continuous nebulized albuterol attenuates acute lung injury in an ovine model of combined burn and smoke inhalation. *Crit Care Med.* **34**, p. 1719–24.
13. van Meer, G., Voelker, D.R., and Feigenson, G.W.,(2008) Membrane lipids: where they are and how they behave. *Nat Rev Mol Cell Biol.* **9**, p. 112–24.
14. Marsh, D.,(2007) Lateral pressure profile, spontaneous curvature frustration, and the incorporation and conformation of proteins in membranes. *Biophys J.* **93**, p. 3884–99.
15. Hannun, Y.A. and Obeid, L.M.,(2008) Principles of bioactive lipid signalling: lessons from sphingolipids. *Nat Rev Mol Cell Biol.* **9**, p. 139–50.
16. Wu, D. and Meydani, S.N.,(2008) Age-associated changes in immune and inflammatory responses: impact of vitamin E intervention. *J Leukoc Biol.* 84, p. 900–14
17. Teichgraber, V., Ulrich, M., Endlich, N., Riethmuller, J., Wilker, B., De Oliveira-Munding, C.C., van Heeckeren, A.M., Barr, M.L., von Kurthy, G., Schmid, K.W., Weller, M., Tummler, B., Lang, F., Grassme, H., Doring, G., and Gulbins, E.,(2008) Ceramide accumulation mediates inflammation, cell death and infection susceptibility in cystic fibrosis. *Nat Med.* **14**, p. 382–91.
18. Jobe, A.H. and Ikegami, M.,(2001) Biology of surfactant. *Clin Perinatol.* **28**, p. 655–69, vii–viii.
19. Orgeig, S., Daniels, C.B., Johnston, S.D., and Sullivan, L.C.,(2003) The pattern of surfactant cholesterol during vertebrate evolution and development: does ontogeny recapitulate phylogeny? *Reprod Fertil Dev.* **15**, p. 55–73.
20. Panda, A.K., Nag, K., Harbottle, R.R., Rodriguez-Capote, K., Veldhuizen, R.A., Petersen, N.O., and Possmayer, F.,(2004) Effect of acute lung injury on structure and function of pulmonary surfactant films. *Am J Respir Cell Mol Biol.* **30**, p. 641–50.
21. Gunasekara, L., Schurch, S., Schoel, W.M., Nag, K., Leonenko, Z., Haufs, M., and Amrein, M.,(2005) Pulmonary surfactant function is abolished by an elevated proportion of cholesterol. *Biochim Biophys Acta.* **1737**, p. 27–35.
22. Ingold, K.U., Webb, A.C., Witter, D., Burton, G.W., Metcalfe, T.A., and Muller, D.P.,(1987) Vitamin E remains the major lipid-soluble, chain-breaking antioxidant in human plasma even in individuals suffering severe vitamin E deficiency. *Arch Biochem Biophys.* **259**, p. 224–5.
23. Traber, M.G., Frei, B., and Beckman, J.S.,(2008) Vitamin E revisited: do new data validate benefits for chronic disease prevention? *Curr Opin Lipidol.* **19**, p. 30–8.
24. Traber, M.G.,(2005) Vitamin E, in *Modern Nutrition in Health and Disease*, (Shils, M.E.,

Olson, J.A., Shike, M., and Ross, A.C., eds.), Lippincott Williams & Wilkins: Baltimore. p. 396–411.

25. Cross, C.E., van der Vliet, A., O'Neill, C.A., Louie, S., and Halliwell, B.,(1994) Oxidants, antioxidants, and respiratory tract lining fluids. *Environ Health Perspect.* 102 Suppl 10, p. 185–91.
26. Bouhafs, R.K. and Jarstrand, C.,(1999) Phagocyte-induced lipid peroxidation of lung surfactant. *Pediatr Pulmonol.* **27**, p. 322–7.
27. Bouhafs, R.K. and Jarstrand, C.,(1999) Lipid peroxidation of lung surfactant by bacteria. *Lung.* **177**, p. 101–10.
28. Atkinson, J., Epand, R.F., and Epand, R.M.,(2008) Tocopherols and tocotrienols in membranes: a critical review. *Free Radic Biol Med.* **44**, p. 739–64.
29. Cuschieri, J., Bulger, E., Biligren, J., Garcia, I., and Maier, R.V.,(2007) Vitamin E inhibits endotoxin-mediated transport of phosphatases to lipid rafts. *Shock.* **27**, p. 19–24.
30. Barbas, C., Castro, M., Bonet, B., Viana, M., and Herrera, E.,(1997) Simultaneous determination of vitamins A and E in rat tissues by high-performance liquid chromatography. *J Chromatogr A.* **778**, p. 415–20.
31. Ito, Y., Ochiai, J., Sasaki, R., Suzuki, S., Kusuhara, Y., Morimitsu, Y., Otani, M., and Aoki, K.,(1990) Serum concentrations of carotenoids, retinol, and alpha-tocopherol in healthy persons determined by high-performance liquid chromatography. *Clin Chim Acta.* **194**, p. 131–44.
32. Podda, M., Weber, C., Traber, M.G., and Packer, L.,(1996) Simultaneous determination of tissue tocopherols, tocotrienols, ubiquinols, and ubiquinones. *J Lipid Res.* **37**, p. 893–901.
33. Ikenoya, S., Abe, K., Tsuda, T., Yamano, Y., Hiroshima, O., Ohmae, M., and Kawabe, K.,(1979) Electrochemical detector for high-performance liquid chromatography. II. Determination of tocopherols, ubiquinones and phylloquinone in blood. *Chem Pharm Bull (Tokyo).* **27**, p. 1237–44.
34. Leonard, S.W., Gumpricht, E., Devereaux, M.W., Sokol, R.J., and Traber, M.G.,(2005) Quantitation of rat liver vitamin E metabolites by LC–MS during high-dose vitamin E administration. *J. Lipid. Res.* **46**, p. 1068–75.
35. Leonard, S.W., Bruno, R.S., Paterson, E., Schock, B.C., Atkinson, J., Bray, T.M., Cross, C.E., and Traber, M.G.,(2003) 5-nitro-gamma-tocopherol increases in human plasma exposed to cigarette smoke in vitro and in vivo. *Free Radic Biol Med.* **35**, p. 1560–7.
36. Galli, F., Lee, R., Dunster, C., and Kelly, F.J.,(2002) Gas chromatography mass spectrometry analysis of carboxyethyl-hydroxychroman metabolites of alpha- and gamma-tocopherol in human plasma. *Free Radic Biol Med.* **32**, p. 333–40.
37. Saito, Y., Yoshida, Y., Nishio, K., Hayakawa, M., and Niki, E.,(2004) Characterization of cellular uptake and distribution of vitamin E. *Ann N Y Acad Sci.* **1031**, p. 368–75.
38. Panin, L.E., Polyakov, L.M., Kolosova, N.G., Russkikh, G.S., and Poteryaeva, O.N.,(1998) Distribution of tocopherol and apolipoprotein A-I immunoreactivity in rat liver chromatin. *Membr Cell Biol.* **11**, p. 631–40.
39. Kiss, E., Nagy, P., Balogh, A., Szollosi, J., and Matko, J.,(2008) Cytometry of raft and caveola membrane microdomains: from flow and imaging techniques to high throughput screening assays. *Cytometry A.* **73**, p. 599–614.
40. Gombos, I., Steinbach, G., Pomozi, I., Balogh, A., Vamosi, G., Gansen, A., Laszlo, G., Garab, G., and Matko, J.,(2008) Some new faces of membrane microdomains: a complex confocal fluorescence, differential polarization, and FCS imaging study on live immune cells. *Cytometry A.* **73**, p. 220–9.
41. Biro, A., Cervenak, L., Balogh, A., Lorincz, A., Uray, K., Horvath, A., Romics, L., Matko, J., Fust, G., and Laszlo, G.,(2007) Novel anticholesterol monoclonal immunoglobulin G antibodies as probes and potential modulators of membrane raft-dependent immune functions. *J Lipid Res.* **48**, p. 19–29.
42. Touboul, D., Brunelle, A., Halgand, F., De La Porte, S., and Laprevote, O.,(2005) Lipid imaging by gold cluster time-of-flight secondary ion mass spectrometry: application to Duchenne muscular dystrophy. *J Lipid Res.* **46**, p. 1388–95.
43. Beattie, J.R., Bell, S.E.J., Borgaard, C., Fearon, A., and Moss, B.W.,(2006) Prediction of adipose tissue composition using Raman spectroscopy: Average properties and individual fatty acids. *Lipids.* **41**, p. 287–294.
44. Beattie, J.R., Bell, S.E.J., Borgaard, C., Fearon, A.M., and Moss, B.W.,(2004) Multivariate prediction of clarified butter composition using Raman spectroscopy. *Lipids.* **39**, p. 897–906.
45. Hancewicz, T.M. and Petty, C.,(1995) Quantitative analysis of vitamin A using Fourier transform Raman spectroscopy. *Spectroc Acta Pt A-Molec Biomolec Spectr.* **51**, p. 2193–2198.
46. Schulz, H. and Baranska, M.,(2007) Identification and quantification of valuable plant substances by IR and Raman spectroscopy. *Vib Spectrosc.* **43**, p. 12–25.

47. Beattie, J.R., Bell, S.E., and Moss, B.W.,(2004) A critical evaluation of Raman spectroscopy for the analysis of lipids: fatty acid methyl esters. *Lipids.* **39**, p. 407–19.
48. Bunow, M.R. and Levin, I.R.,(1977) Raman spectra and vibrational assignments for deuterated membrane lipids. 1,2 dipalmitoyl phoshatisylcholine-d_9 and d_{62}. *Biochim Biophys Acta.* **489**, p. 191–206.
49. Kint, S., Wermer, P.H., and Scherer, J.R.,(1992) Raman-Spectra of hydrated phospholipid-bilayers 2. Water and headgroup interactions. *J Phys Chem.* **96**, p. 446–452.
50. Lawson, E.E., Anigbogu, A.N.C., Williams, A.C., Barry, B.W., and Edwards, H.G.M.,(1998) Thermally induced molecular disorder in human stratum corneum lipids compared with a model phospholipid system; ft-Raman spectroscopy. *Spectrochim Acta A-Mol Biomol Spectros.* **54**, p. 543–558.
51. Wallach, D.F.H., Verma, S.P., and Fookson, J.,(1979) Application of laser Raman and infrared spectroscopy to the analysis of membrane structure. *Biochim Biophys Acta.* **559**, p. 153–208.
52. Beattie, J.R., Brockbank, S., McGarvey, J.J., and Curry, W.J.,(2005) Effect of excitation wavelength on the Raman spectroscopy of the porcine photoreceptor layer from the area centralis. *Mol Vis.* **11**, p. 825–832.
53. Haka, A.S., Volynskaya, Z., Gardecki, J.A., Nazemi, J., Lyons, J., Hicks, D., Fitzmaurice, M., Dasari, R.R., Crowe, J.P., and Feld, M.S.,(2006) In vivo margin assessment during partial mastectomy breast surgery using Raman spectroscopy. *Cancer Res.* **66**, p. 3317–3322.
54. Min, Y.K., Yamamoto, T., Kohda, E., Ito, T., and Hamaguchi, H.,(2005) 1064 nm near-infrared multichannel Raman spectroscopy of fresh human lung tissues. *J Raman Spectrosc.* **36**, p. 73–76.
55. Lajoie, P. and Nabi, I.R., (2007) Regulation of raft-dependent endocytosis. *J Cell Mol Med.* **11**, p. 644–53.
56. Eriksson, L., Johansson, E., Kettaneh-Wold, N., Trygg, J., Wikström, C., and Wold, S., eds. *Multi- and Megavariate Data Analysis Part I: Basic Principles and Applications, Second revised and enlarged edition* 2nd ed. Vol. 1. 2006, Umetrics: Umea. p. 425.
57. Eriksson, L., Johansson, E., Kettaneh-Wold, N., Trygg, J., Wikström, C., and Wold, S., eds. *Multi- and Megavariate Data Analysis Part II: Advanced Applications and Method Extensions, Second revised and enlarged edition* 2nd ed. Vol. 2. 2006, Umetrics: Umea. 345.
58. McCreery, R.L.,(2000) Raman Spectroscopy for Chemical Analysis. 1 ed. *in Chemical Analysis: a Series of Monographs of Analytical Chemistry and its Applications.*, (Winefordner, J.D., ed). Wiley, New York.
59. Tu, A.T.,(1982) *Raman Spectroscopy in Biology: Principles and Applications.* Wiley, New York.
60. Bell, S.B., JR; McGarvey, J.J.; Peters, K L., Sirimuthu, N.M.S., Speers, S J.,(2004) Development of sampling methods for Raman analysis of solid dosage forms of therapeutic and illicit drugs. *J Raman Spectrosc.* **35**, p. 409–417.
61. Glenn, J.V., Beattie, J.R., Barrett, L., Frizzell, N., Thorpe, S.R., Boulton, M.E., McGarvey, J.J., and Stitt, A.W.,(2007) Confocal Raman microscopy can quantify advanced glycation end product (AGE) modifications in Bruch's membrane leading to accurate, nondestructive prediction of ocular aging. *FASEB J.* **21**, p. 3542–52.
62. Beattie, J.R., Glenn, J.V., Boulton, M.E., Stitt, A.W., and McGarvey, J.J.,(2009) Effect of signal intensity normalization on the multivariate analysis of spectral data in complex 'real-world' datasets. *J Raman Spectrosc.* **40**, p. 429–435.
63. Jirasek, A., Schulze, G., Yu, M.M.L., Blades, W., and Turner, R.F.B.,(2004) Accuracy and precision of manual baseline determination. *Appl Spectrosc.* **58**, p. 1488–1499.
64. Lieber, C.A. and Mahadevan-Jansen, A.,(2003) Automated method for subtraction of fluorescence from biological Raman spectra. *Appl Spectrosc.* **57**, p. 1363–1367.